4

Rare-Earth-Doped Low Phonon Energy Halide Crystals for Mid-Infrared Laser Sources

M. Velázquez[1], A. Ferrier[2], J.-L. Doualan[3] and R. Moncorgé[3]
[1]*CNRS, Université de Bordeaux, ICMCB, Pessac*
[2]*LCMCP,CNRS-Université de Paris 6-Collège de France-Paris Tech,Paris*
[3]*CIMAP, CEA-CNRS- ENSICaen-Université de Caen, Caen*
France

1. Introduction

Since ~15 years, solid state lasers emitting in bands II (2.7-4.3, 4.5-5.2 μm) and III (8-14 μm) of the atmosphere transparency spectral range are being developed for imaging, polluting species detection as well as military NRBC detection and optronic countermeasures. Because most of these applications require highly brilliant and/or important peak power laser sources, several RE^{3+}-doped (RE=rare earth) low phonon energy ($\hbar\omega$<400 cm^{-1}) chloride and bromide crystals, such as APb_2X_5 (A=K,Rb;X=Cl,Br) or $CsCdBr_3$, stand out as promising laser gain media in the mid-infrared (MIR) spectral range [Doualan & Moncorgé, 2003; Isaenko et al., 2008]. Indeed, these bulk crystals, transparent up to more than 18 μm, could be used at room temperature and their emission lifetime-emission cross section product ($\sigma_{EM}\tau_R$) at the laser wavelength is high enough to allow for energy storage and subsequent pulsed regime laser operation. Moreover, in these systems, the laser beam quality could be high even at high output powers.

This chapter is composed of three parts. The first one reviews all the successful laser operations ever demonstrated. The basic thermal, mechanical, optical and spectroscopical properties characterizations are presented for a series of halide crystals : single crystal Raman spectroscopy, Fourier-transformed infrared (FTIR) spectroscopy, X-Ray diffraction (XRD) and thermal conductivity data, showing at a glance the transparency range, the highest phonon energies, the site symmetry of RE^{3+} ions as well as mechanical hardness, among other laser-related characteristics. The second part deals with RE^{3+} ions spectroscopy related to the pumping strategy for a better inversion population kinetics at play during laser operation. Such mechanisms as upconversion energy transfers (ETU) and excited-state absorption (ESA) are detailed in the case of Er^{3+} and Pr^{3+} ions. Spectroscopic data on more exotic Tl_3PbX_5 (X=Cl,Br) crystals, which are optically non linear in addition to the general propensity to MIR laser operation is presented only to illustrate crystal field strength trends affecting the absorption and emission bands, as well as energy transfer mechanisms between Er^{3+} ions and ultimately gain cross sections. The third part of this chapter addresses the synthesis and crystal growth of pure and RE-doped chlorides and bromides in relation to their spectroscopical and laser operation properties. The choice of such growth parameters as the nature and shape of the crucible, the nature of the gas and its pressure, the

growth rate, is fundamental to avoid bubble formation, stabilize RE^{3+} oxidation state, minimize the complications arising from crystallographic phase transition and the mechanical stresses upon cooling, control as much as possible RE^{3+}-ion segregation, and so on. All these aspects ultimately affect laser operation and the relationships between growth conditions, growth defects and laser performances have scarcely been discussed in the literature on these laser materials, which is surprising if these crystals are to be produced on a large industrial scale by the well spread Bridgman-Stockbarger method.

2. MIR solid state laser operation

To date, the longest laser wavelength ever achieved, 7.15 µm [Bowman et al., 1994, 1996], has been obtained with a 4-mm long $LaCl_3:Pr^{3+}$ (0.7 % at.) single crystal operated in the pulsed regime. This pioneering work by Bowman and his collaborators has not been reproduced since 1996, probably because the crystals were so hygroscopic that they had to be kept in a cryostat during all the measurements to avoid their deliquescence. In these crystals, the most energetic phonon vibrates at 210 cm^{-1} and the transparency range extends up to 15 µm. The pumping scheme of this laser emission involves an ETU mechanism by photon addition from the thermalized $^3H_6$ and $^3F_2$ levels according to $2*^3H_6 \rightarrow {}^3H_5+{}^3F_3$ (figure 1). The laser crystal is pumped at 2.02 µm on the $^3F_2$ level by means of a Tm:YAG laser (being itself diode- or flashlamp-pumped) delivering free-running pulse trains at frequencies from 2 to 100 kHz with an average power 70 W. In spite of this "awkward and expensive 2 µm pumping scheme", as Howse *et al.* recently put it [Howse et al., 2010], the crystal exhibits a high absorption cross section around 2 µm (10 times higher, for instance, than the absorption one around 800 nm, which corresponds to the $^4I_{9/2}$ pump level of $Er^{3+}:KPb_2Cl_5$, figures 2 and 3). The laser emission centered at 7.15 µm occurs between levels $^3F_3$ (the experimental lifetime of which τ_2, measured by direct pumping with an Er^{3+} laser at 1.6 µm, equals 58 µs) and $^3F_2$. At 20 °C, the laser slope efficiency reaches 3.9 %, the absorbed power conversion yield 2.3 % and the pump threshold ~4 mJ. Bowman *et al.* suggested that thermalization of levels $^3F_4$ and $^3F_3$ would make efficient a direct pumping at 1.5 µm on level

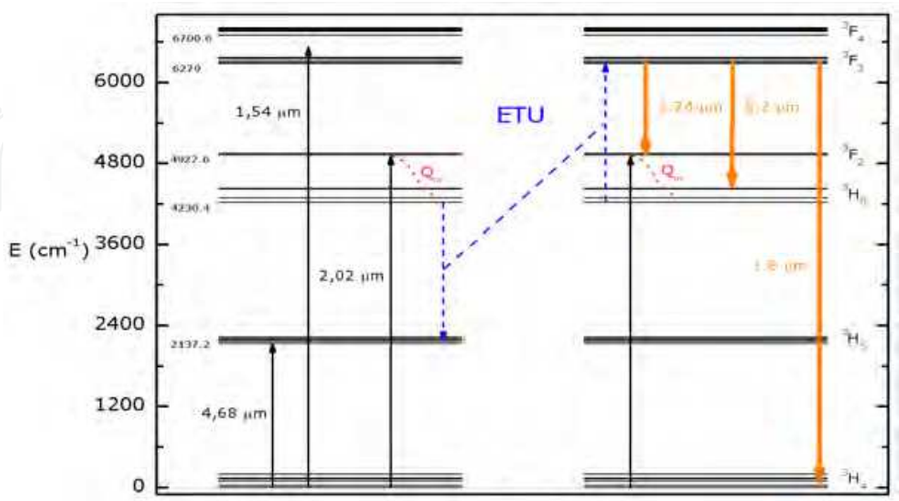

Fig. 1. Energy level diagram of Pr^{3+} ions in the $LaCl_3$ host crystal. Blue arrows indicate the phonon assisted non radiative ETU mechanism.

$^3F_4$ (figure 1). They were also the first to tune laser operation from 4.42 to 4.70 µm on the $^4I_{9/2} \rightarrow {}^4I_{11/2}$ transition of Er^{3+} ions in KPb_2Cl_5 single crystals, with diode pumping at 800 nm and an absorbed power conversion yield at room temperature of 7.6 % (to be compared with the quantum yield of 17.4 %) [Bowman et al., 1999, 2001; Condon et al., 2006a] (see in Fig. 2).

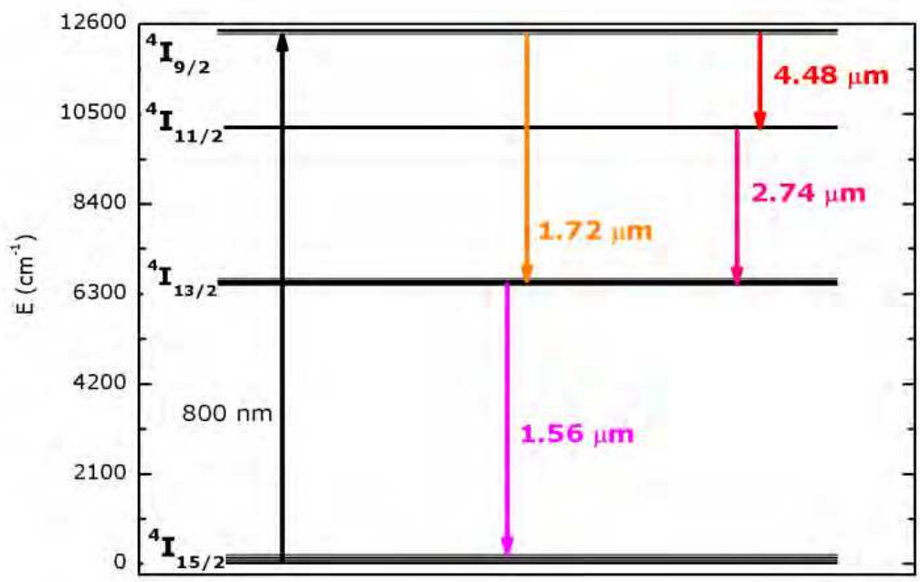

Fig. 2. Four first energy levels diagram of Er^{3+} ions in Tl_3PbBr_5 and their experimental lifetimes.

The main reason why the APb_2X_5 (A=K,Rb;X=Cl,Br) family of laser hosts has triggered a continuous breed of publications since 2001 lies in the non hygroscopicity of the crystals, which turns out to be unusual among chlorides and bromides host crystals with luminescent properties [Egger at al., 1999; Kaminska et al., 2011; Nitsch et al., 1993, 1995a, 1995b, 2004; Nitsch & Rodová 1999; Riedener et al., 1997; Rodová et al., 1995; Vinogradova et al., 2005; Zhou et al., 2000]. The interest of diode pumping lies in the simple and compact cavity design (cavity length of 8 mm with $KPb_2Cl_5:Er^{3+}$ crystals), and that of KPb_2Cl_5 crystals, as previously stated, to manipulate a non hygroscopic and air stable gain medium. Even if a 19 W power diode had to be used (absorption rate ~4 %) with a beam waist ~150 µm, it should be noted that this crystal was efficiently operated at ~50 Hz, without any cooling system, clearly establishing its satisfying thermomechanical properties (table 1). Laser operation was demonstrated at 5.5 µm in $RbPb_2Cl_5$ crystals doped with Dy^{3+} ions (2.10^{19} cm^{-3}, $^6H_{9/2}+{}^6F_{11/2} \rightarrow {}^6H_{11/2}$), with flash-lamp pumped YAG:Nd^{3+} laser operating in free multimode simultaneously at 1.32 and 1.34 µm, with a repetition rate of 2.5 Hz and a beam waist in the crystal ~300 µm [Okhrimchuk et al., 2007]. Preliminary laser tests on unoriented crystals obviously full of scattering defects gave a laser slope ~0.1 % and a threshold of 25 mJ. Although Dy^{3+} ion spectroscopy were investigated in $CaGaS_4$ and KPb_2Cl_5 crystals, because of their seemingly promising laser transitions $^6H_{11/2} \rightarrow {}^6H_{13/2}$ at 4.31 µm, we shall not insist on that since they can not be currently diode pumped at 1.32 µm [Nostrand et al., 1998, 1999; Okhrimchuk, 2008].

Properties	KPb_2Cl_5	$RbPb_2Cl_5$	KPb_2Br_5	Tl_3PbBr_5	$CsCdBr_3$
Structure, space group	Monoclinic, $P2_1/c$	Monoclinic, $P2_1/c$	Monoclinic, $P2_1/c$	Orthorhombic, $P2_12_12_1$	Hexagonal, $P6_3/mmc$
Cell parameters (Å)	a=7.919 Å b=8.851 Å c=12.474 Å β=90.13 °	a=8.959 Å b=7.973 Å c=12.492 Å β=90.12 °	a=9.256 Å b=8.365 Å c=13.025 Å β=90.00(3) °	a=15.395 Å b=9.055 Å c=8.544 Å	a=7.681 Å c=6.726 Å
Z	4	4	4	4	2
Volumic mass ($g.cm^{-3}$)	4.629	5.041	5.619	6.80	4.77
RE^{3+} substitution site density (cm^{-3})	Pb^{2+}, C_1, 4.6×10^{21} (*)	unknown, C_1, 4.5×10^{21} (*)	unknown, C_1, 4.0×10^{21} (*)	unknown, C_1, 3.4×10^{21}	Cd^{2+}, D_{3d} (C_{3v} with charge compensation) 5.8×10^{21}
Thermal conductivity at room temperature ($W.m^{-1}.K^{-1}$)	4.62	4			0.3
Young moduli (GPa)	E_1~29.9 E_2~24.9 E_3~27.0				$E_1=E_2$~22.2 E_3~29.4
Shear moduli (GPa)	G_{44}~11 G_{55}~11.1 G_{66}~14.3				$G_{44}=G_{55}$~4.5 G_{66}~7.7
Hardness (Mohs)	2.5	2.5	2.5	2 502 MPa	294 Mpa
Thermal expansion coefficients (10^{-6} K^{-1})	α_a=38.6 α_b=42.6 α_c=39.3	α_a=26 α_b=36 α_c=33	α_a=40 α_b=36 α_c=28	α_a=41 α_c=62	
Maximum phonon frequency (cm^{-1})	204.8	203	138	137.5	161
Transparency range (μm)	0.3-20	0.37-20	0.4-30	0.4->24	0.28-35
Energy bandgap (eV)	4.79	4.83	4.12		~3.5-4
Refractive index	n_x=1.9406 n_y=1.9466 n_z=1.9724 (@ 1 μm)	n=2.019 (@ 0.63 μm)	n_x=2.191 n_y=2.189 n_z=2.247 (@ 0.63 μm)	n~2.23 (@ 0.63 μm)	1.76 (@ 1 μm)
Thermo-optic coefficient (10^{-5} K^{-1}, @ 1 μm)	-7.0 -10.0 -10.5		-13.0 -14.1 -14.9		
Er^{3+}-doped crystals (figure 2)					
Absorption cross section around 800-810 nm (10^{-21} cm^2)	2.4			2.9	

$^4I_{9/2}$ experimental lifetime (ms)	2.62		1.2 or 1.9	1.8	10.7
$^4I_{9/2}\rightarrow{}^4I_{11/2}$ branching ratio (%)	1.2				
$^4I_{11/2}$ experimental lifetime (ms)	3.23		2.1	3.1	
Emission cross section around 4.4-4.6 μm (10^{-21} cm²)	2			2.1	
$\sigma_{EM}\tau_{exp}$ around 4.4-4.6 μm (10^{-24} cm².s)	5.2			3.6	
$C_{DD}(^4I_{9/2},{}^4I_{15/2})\rightarrow(^4I_{15/2},{}^4I_{9/2})$ (10^{-40} cm⁶.s^{-1})	1.19			0.95	
$C_{DA}(^4I_{9/2},{}^4I_{11/2})\rightarrow(^4I_{15/2},{}^4F_{3/2})$ (10^{-40} cm⁶.s^{-1})	2.54			0.48	P_{DA}=1942 s^{-1}
$C_{DA}(^4I_{9/2},{}^4I_{13/2})\rightarrow(^4I_{15/2},{}^4S_{3/2})$ (10^{-40} cm⁶.s^{-1})	1			0.44	
Auzel crystal field parameter (cm^{-1})	1771 (C_s/C_2)			1327 (C_s/C_2)	1502 (C_{3v})
Pr^{3+}-doped crystals (figure 1)					
Absorption cross section around 2 μm (10^{-20} cm²)	3.5		4.6	1.9	5.5
$^3F_3$ experimental lifetime (ms)	0.362	0.11	0.3	0.89	1.57
$(^3F_4,{}^3F_3)\rightarrow{}^3F_2$ branching ratio (%)	ε			ε	ε
$^3F_2$ experimental lifetime (ms)	0.95	1	1.5	3.1	3.6
$^3H_5$ experimental lifetime (ms)	4.5	5	26.5	42.2	27.5
Emission cross section around 4.6-4.8 μm (10^{-21} cm²)	4.8		4	5.4	3.2
$\sigma_{EM}\tau_{exp}$ around 4.6-4.8 μm (10^{-23} cm².s)	2.2		10.6	22.8	8.8
Auzel crystal field parameter (cm^{-1})	1746 (C_s/C_2)				4968 (C_{3v})

Table 1. Laser-related crystallographic, thermal, mechanical, optical and spectroscopical properties of selected low phonon energy halide crystals [Aleksandrov et al., 2005; Atuchin et al., 2011; Cockroft et al., 1992; Doualan & Moncorgé, 2003; Ferrier et al., 2006a, 2007, 2008a, 2008b, 2009a, 2009b; Heber et al., 2001; Isaenko et al., 2008, 2009a, 2009b; Malkin et al., 2001; Mel'nikova et al., 2005; Merkulov et al., 2005; Neukum et al., 1994; Nostrand et al., 2001; Okhrimchuk et al., 2006; Popova et al., 2001; Quagliano et al., 1996; Ren et al., 2003; Singh et al., 2005; Velázquez et al., 2006a, 2006b; Virey et al., 1998; Vtyurin et al., 2004, 2006]. (*) per lead type of crystallographic site.

3. Spectroscopic parameters for laser operation

3.1 Er^{3+}-doped single crystals

The great number of close energy levels within the 4f configuration explains the interest for RE ions as optically active species for MIR applications. When dissolved in low phonon energy crystals such as halides and bromides, nonradiative multiphonon emission probabilities between the two levels of the laser transition are significantly reduced. Hence, they allow for reaching long emitting level lifetimes, on the order of a few tens of µs to tens of ms. Consequently, RE-doped APb_2X_5 crystals are likely to insure sufficient energy storage for amplification. The shape and magnitude of the absorption bands around 800 and 980 nm (figure 3), where efficient, compact, rugged, high-powered and cheap laser diodes are easily available as pumping sources, has been widely characterized. The forced electric dipole emission bands from the Er^{3+} ions $^4I_{9/2}$ multiplet, which are never obtained in the MIR range (1.7 µm, 4.5 µm) in oxides and fluorides, was also exhaustively discussed (figure 4). On the other hand, energy transfers between Pr^{3+} ions (figure 1), on which the world record in terms of laser wavelength is based, has been investigated with an emphasis put on ion pairing effects, by comparing the efficiency of energy transfers in KPb_2Cl_5, Tl_3PbBr_5 and $CsCdBr_3$, all of which being non hygroscopic. Exactly as in the case of Er^{3+} ions, the shape, magnitude and possible polarization effects of the absorption and emission bands involved in laser operation around 5 µm have been commented and compared to well established laser systems in the near infrared such as Nd^{3+}:YAG.

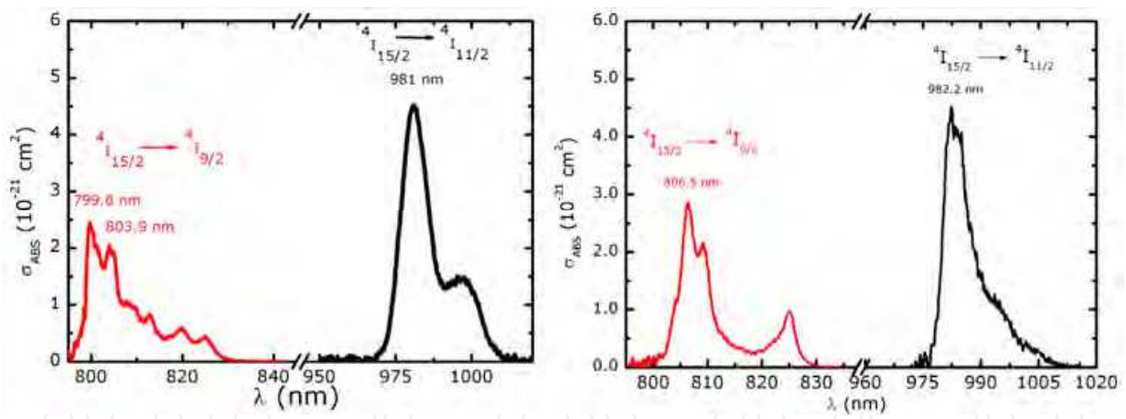

Fig. 3. Room temperature absorption cross section around 800 and 980 nm, left : $KPb_2Cl_5:Er^{3+}$; right : $Tl_3PbBr_5:Er^{3+}$.

Absorption (or transmission), emission and excitation spectra recorded as a function of temperature at low temperature (10-50 K) over a broad spectral range allow for accurately determining (±3 cm^{-1}) the crystal-field energy sublevels of Er^{3+} ions dissolved into KPb_2Cl_5 and Tl_3PbBr_5 and fitting the energy level structure with parameterized crystal-field model Hamiltonians. This makes possible, among other things :

- to calculate the electronic sum over states function of the first 11 multiplets (from $^4I_{15/2}$ to $^2H_{9/2}$)
- to characterize the possible existence of several incorporation sites for RE ions

The knowledge of these data is mandatory not only to estimate absorption and emission cross sections of the optical lines exploited for laser operation, but also to assign the bands observed on the excitation and anti-Stokes emission spectra. This has given a strong impetus to spectroscopic investigations in Russia, in Europe and in the USA [Balda et al., 2004; Gruber et al., 2006; Jenkins et al., 2003; Quimby et al., 2008; Tkachuk et al., 2005, 2007]. The peak-by-peak assignment of crystal-field sublevels also permits to check the number of peaks expected for a complete degeneracy lift of each multiplet (J+1/2). This demonstrates the occurrence of only one symmetry-type site for Er^{3+} ions in these two host compounds, *a priori* C_1 (table 1). However, as a great number of non equivalent defects is likely to form (for instance, more than one hundred in KPb_2Cl_5 [Velázquez et al., 2006b]) and the point group symmetry is very low for all the atomic positions, the precise characterization of the Er^{3+} incorporation sites in both compounds remains difficult. Crystal-field calculations with C_s/C_2 point groups lead to a satisfactory agreement between experimental and calculated energy levels [Ferrier et al., 2007, 2008a; Gruber et al., 2006].

Absorption cross sections around 800 and 980 nm, spectral range in which diode pumping is commonly available, are shown in figure 3. The absorption bands are large (for a RE^{3+}-doped system) and so suitable for diode pumping. Judd-Ofelt analysis performed with absorption spectra over the first 11 excited states showed that the branching ratio of the $^4I_{9/2} \rightarrow {}^4I_{11/2}$ transition around 4.5 μm amounts to only 1.2 %. But even if this is low as compared to other laser systems, these absorption cross sections are typical of forced electric dipole transitions and sufficient to be exploited under diode pumping [Bowman et al., 1999, 2001; Condon et al., 2006a], provided that a high power is used. Cross section calibrated emission spectra obtained under excitation at 800 nm display a poorly structured and virtually independent on polarization broad band, which exemplifies the interest in chlorides and bromides for MIR laser applications (figure 4).

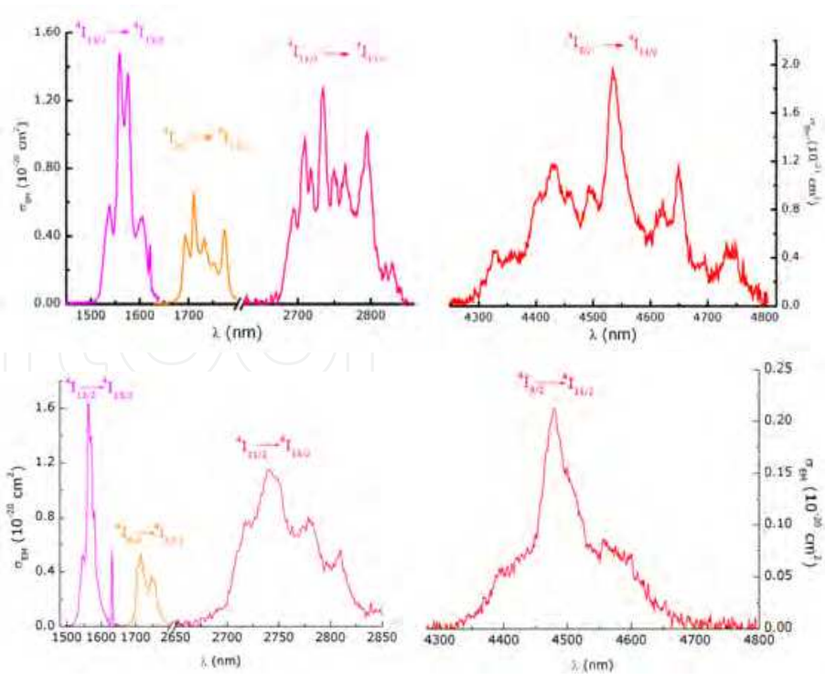

Fig. 4. Er^{3+} ions emission spectra in KPb_2Cl_5 (top) and in Tl_3PbBr_5 (bottom) at room temperature, under cw excitation by Sa:Ti laser at 800 nm.

Indeed, emissions from multiplet $^4I_{9/2}$, to multiplet $^4I_{13/2}$ at 1.7 μm, and to multiplet $^4I_{11/2}$ at 4.5 μm are never observed neither in oxides nor in fluorides. In particular, in $Tl_3PbBr_5:Er^{3+}$, 15 « Raman » phonons of the highest energy are required to match the energy difference between the two multiplets implied in the laser transition $^4I_{9/2}\rightarrow{}^4I_{11/2}$, which entails multiphonon emission kinetics much slower than radiative de-excitation ones (figure 2).

Emission cross-sections, ~2.10^{-21} cm² ($\sigma_{EM}\tau_R$~(3-5).10^{-24} cm².s at λ_{max}~4.5 μm), are as high in Tl_3PbBr_5 as in KPb_2Cl_5, and the experimental lifetimes of the three first excited levels 2 to 4 ms in both compounds, which is favourable to diode pumped pulsed regime laser operation. As the experimental lifetime of the terminal level (more than 3 ms) is longer than that of the emitting one (around 2 ms), we investigated the possibility of observing anti-Stokes emissions at room temperature and recording their excitation spectra likely to unveil parasitic mechanisms depleting $^4I_{9/2}$ and $^4I_{11/2}$ energy levels. Figure 5 shows the anti-Stokes luminescence issued from $^4G_{11/2}$, $^2H_{9/2}$ (violet), $^4F_{3/2}$/$^4F_{5/2}$ (blue), $^2H_{11/2}$, $^4S_{3/2}$ (green), $^4F_{9/2}$ and $^2H_{11/2}$ (red) by Ti:Sa laser cw excitation at 804 nm, in Er^{3+}-doped KPb_2Cl_5 and Tl_3PbBr_5 crystals. In order to understand by which mechanism(s), likely to affect population inversion kinetics during laser operation, all these levels gets populated in spite of the fact that excitation around 800 nm is non resonant, it proved useful to get excitation spectra of these emissions as well as fluorescence decay measurements under pulsed non resonant excitation. References [Balda et al., 2004; Ferrier et al., 2007, 2008a; Quimby et al., 2008; Tkachuk et al., 2007] highlight the relevance of such processes as :

- excited state absorption $^4I_{9/2}\rightarrow{}^2H_{9/2}$ from 816 to 837 nm (σ_{ESA}~(2-3).10^{-21} cm²), $^4I_{11/2}\rightarrow(^4F_{3/2},^4F_{5/2})$ at 815 and 839 nm (σ_{ESA}~(1-1.5)×10^{-20} cm²) and $^4I_{13/2}\rightarrow(^2H_{11/2},^4S_{3/2})$ around 800 and 847 nm (σ_{ESA}~(3-4).10^{-21} cm²) ;
- resonant energy transfers by ETU $2^*{}^4I_{9/2}\rightarrow{}^4I_{15/2}+{}^2H_{9/2}$, $^4I_{11/2}+{}^4I_{9/2}\rightarrow{}^4I_{15/2}+(^4F_{3/2},^4F_{5/2})$ and $2^*{}^4I_{9/2}\rightarrow{}^4I_{13/2}+{}^4S_{3/2}$ around 800 nm (figure 6), the laser pumping wavelength which is foreseen in this system.

In Tl_3PbBr_5 crystals, excited state absorption cross section are virtually the same in magnitude but with a systematic red shift ~5-6 nm. Time resolved emission spectroscopy is mandatory to quantify the different relaxation rates, since population mechanisms of $^2H_{9/2}$ and ($^4F_{3/2}$,$^4F_{5/2}$) levels coexist more or less as a function of the excitation wavelength. Calibration of the spectra in cross sections units by successive application of Fuchtbauer-Ladenburg and MacCumber relationships permits to estimate the energy transfer microparameters which appear in the rate equations driving the population inversion kinetics during laser operation, and consequently to optimize the wavelength and temporal width of pumping pulses. This investigation demonstrated that the effect of ETU (see in Fig. 6) turns out to be completely negligible until the concentration of 3.3 mol % is achieved in KPb_2Cl_5 crystals [Ferrier et al., 2007] (which corresponds to an average Er^{3+}-Er^{3+} distance of ~12 Å), and that optical pumping at 800 nm, that is, at the absorption peak in $KPb_2Cl_5:Er^{3+}$, does not lead to substantial excited state absorption losses towards the $^2H_{9/2}$ level (see in Fig. 5). As a matter of fact, when the Er^{3+} ion concentration increases, losses by ETU also increase, but less rapidly than the population rate of the emitting $^4I_{9/2}$ level, so that the resulting population inversion also increases. A striking structure-property relationship can be seen in the fact that the $^4F_{7/2}$ experimental lifetime is seven to eight times longer in Tl_3PbBr_5 (70 μs) and in KPb_2Br_5 (85 μs) than in KPb_2Cl_5 (10 μs), which demonstrates that non

radiative multiphonon emission kinetics are much slower in bromides than in chlorides [Hömmerich et al., 2005]. Indeed, the $^2H_{11/2}$ level just below the $^4F_{7/2}$ one lies at 1321 (resp. 1296) cm^{-1} in KPb_2Cl_5 (resp. Tl_3PbBr_5), requiring 6.4 (resp. 9.4) phonons of the highest frequency to match this energy difference. Riedener and Güdel [Riedener & Güdel, 1997] have already observed blue and very weak anti-Stokes luminescence in $RbGd_2Br_7:Er^{3+}$ crystals, that was spaced by a few hundreds of cm^{-1} from intense anti-Stokes green luminescence in $RbGd_2Cl_7:Er^{3+}$ crystals. It was obtained under excitation at 977.6 nm in the bromide and at 975.1 nm in the chloride on the $^4I_{11/2}$ level, followed by ESA on the $^4F_{7/2}$ level.

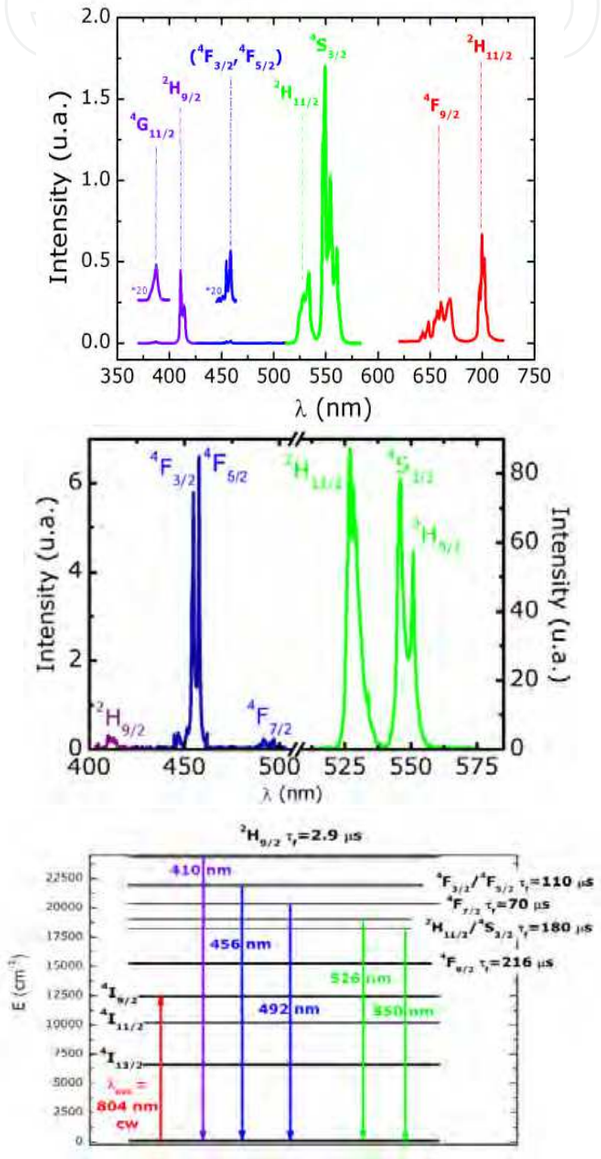

Fig. 5. Top left, anti-Stokes emission spectra of $KPb_2Cl_5:Er^{3+}$ at room temperature under cw excitation at 800 nm ; top right, anti-Stokes luminescence spectra of $Er^{3+}:Tl_3PbBr_5$, transitions from $^2H_{9/2}$ (410 nm), ($^4F_{3/2}$,$^4F_{5/2}$) (456 nm), $^4S_{3/2}$ (550 nm) and $^4I_{13/2}$ (1.55 µm) to $^4I_{15/2}$ under cw excitation at 804 nm. Bottom, energy levels diagram of Er^{3+} ions in Tl_3PbBr_5.

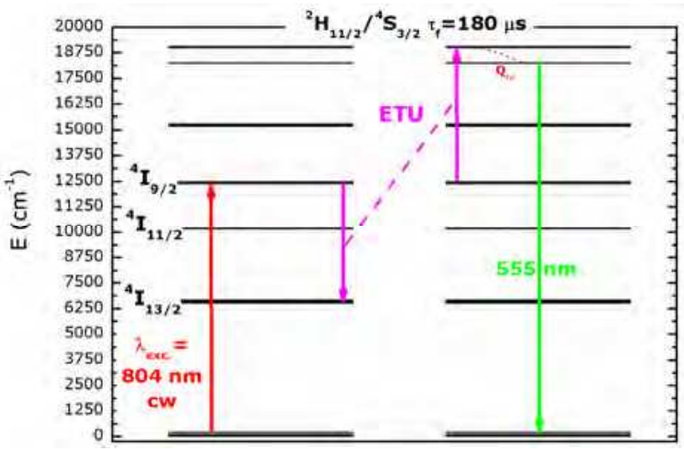

Fig. 6. Green anti-Stokes luminescence of Er^{3+} ions in KPb_2Cl_5 at room temperature, under Sa:Ti laser excitation at 804 nm, and most prominent ETU mechanism.

In addition, the bottleneck effect of the laser effect likely to arise from the long emission lifetime of the $^4I_{13/2}$ level ≈4.6 ms, is unsignificant in pulsed regime because the latter is virtually empty. The gain cross section is displayed in figure 7 and permits the identification of the most probable laser oscillation wavelength at the maxima.

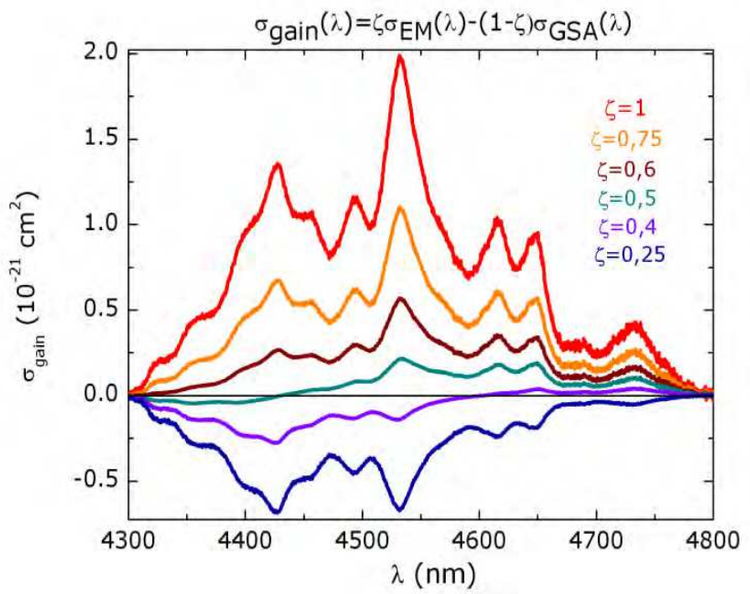

Fig. 7. Gain cross section around 4.5 µm in $KPb_2Cl_5:Er^{3+}$, with $\zeta=n^4I_{9/2}/(n^4I_{9/2}+n^4I_{11/2})$.

3.2 Pr^{3+}-doped single crystals

By adjusting their fluorescence data at 1.6 µm issued from the $^3F_3$ level with the system of population rate equations reported hereafter, Bowman *et al.* could extract the value of the crossed relaxation parameter $\chi \approx 1.3\times10^{-16}$ cm^3.s^{-1} and that of the $(^3F_4,^3F_3)\rightarrow(^3F_2,^3H_6)$ transition branching ratio, $\beta \approx 1\%$:

$$\frac{\partial N_{\left({}^3F_2;{}^3H_6\right)}}{\partial t} = \frac{\beta}{\tau_2} N_{\left({}^3F_4;{}^3F_3\right)} - 2\chi N^2_{\left({}^3F_2;{}^3H_6\right)}$$

$$\frac{\partial N_{\left({}^3F_4;{}^3F_3\right)}}{\partial t} = \chi N^2_{\left({}^3F_2;{}^3H_6\right)} - \frac{N_{\left({}^3F_4;{}^3F_3\right)}}{\tau_2}$$

Moreover, by matching the decay rate to an exponential law, they determined the apparent lifetime $"\tau_2" \approx 900\mu s$ (that is, 15.5 times longer than the real τ_2) standing for the electronic feeding of the $^3F_3$ level due to the crossed relaxation mechanism (figure 1). It is worth noting the laser emission centered at 5.2 μm (figure 1) which is obtained at 130 K with the same pumping scheme, a power conversion yield of 23 % and a threshold of 2 mJ that increases strongly with temperature. Homovalent substitution of La^{3+} cations to Pr^{3+} ones modifies very weakly local vibrational frequencies because there is neither vacancies nor interstitial formation in the vicinity of Pr^{3+} ions and the molar masses are very close (only 1.4 % relative difference). It seems that Pr^{3+} ions form pairs, explaining the efficiency of the energy transfer [Guillot-Noël et al., 2004]. This pionnering work of Bowman and his coworkers triggered the interest for a systematic study of Pr^{3+} ion fluorescence kinetics around 7.2 μm, in host compounds as KPb_2Cl_5, Tl_3PbBr_5 and $CsCdBr_3$, all non hygroscopic, by means of two pumping schemes :

- at 2 μm, with a diode pumped Tm^{3+} laser, on the $^3F_2$ level followed by thermalization and ETU ;
- at 1.5 μm, with an Er^{3+} laser, directly on $^3F_4$ level followed by thermalization.

In the near future, such systems will also be pumped at 4.6 μm by means of high power quantum cascade laser (QCL) diodes for the emission at 5 μm from the $^3H_5$ level, particularly in KPb_2Cl_5 because the pumping strategy involving ETU seems more favourable than in $CsCdBr_3$, not only because of lower phonon energies but also because the one dimensional crystal structure of the latter compounds favours ion pairing of Pr^{3+} [Amedzake et al., 2008; An & May, 2006; Balda et al., 2002, 2003; Bluiett et al., 2008; Chukalina, 2004; Ferrier et al., 2009a, 2009b; Gafurov et al., 2002; Guillot-Noël et al., 2004; Neukum et al., 1994; Rana & Kaseta, 1983]. Absorption and emission spectra recorded as a function of temperature at low temperature (10-50 K) over a broad spectral range allows for the determination of Pr^{3+} ions crystal field sublevels dissolved in KPb_2Cl_5, and to match them with the eigenvalues of a parameterized crystal field model hamiltonian taking into account 74 sublevels of the 12 first multiplets. The $^3P_1$ and $^1I_6$ were not included in the refinement procedure because their crystal field sublevels could not be successfully deconvoluted, even at low temperatures. Absorption cross section peaks around 2 μm are virtually twice higher in $CsCdBr_3$ than in Tl_3PbBr_5 crystals, and the absorption line profiles in $CsCdBr_3$:Pr^{3+} differs from those observed in the two other compounds (figure 8). In the former crystals, absorption lines are narrow and structured, whereas in the latter ones they are broad, consistently with point defect disorders expected for the three crystal structures [Ferrier et al., 2006a; Guillot-Noël et al., 2004; Velázquez et al., 2006b]. The absorption cross section at 1.55 μm is of the same magnitude as that at 2 μm in KPb_2Cl_5 and Tl_3PbBr_5, suggesting the possibility of a direct pumping on the ($^3F_4$,$^3F_3$) levels with an Er^{3+} Kigre laser (or any other means : fibre, IR laser diode, etc.). Crystal field calculations with point symmetry C_s/C_2 lead to a good agreement between experimental and simulated energy

levels [Ferrier et al., 2008b]. Figure 1 allows for checking the many possible resonances around 2.1 µm, between $^3H_4$, $^3H_5$, ($^3F_2$,$^3H_6$) and ($^3F_4$,$^3F_3$) levels, propicious to efficient energy transfers (even at low Pr^{3+} ions concentration) which make difficult the resolution of the emission spectra and the interpretation of the relaxation kinetics of these complex excitations. Fluorescence decay measurements, from the $^3F_3$ level after excitation at 1.54 µm, realized on weakly (~5.10^{18} ions.cm^{-3}) and « strongly » (~5.31×10^{19} ions.cm^{-3}) Pr^{3+}-doped KPb_2Cl_5 crystals, revealed an exponential decay in the first case, and non exponential in the second one, firmly establishing energy transfers with concentration such as : $^3H_4 + {}^3F_3 \rightarrow {}^3H_5 + {}^3H_6$ and $^3H_5 + {}^3F_3 \rightarrow 2^*{}^3H_6$.

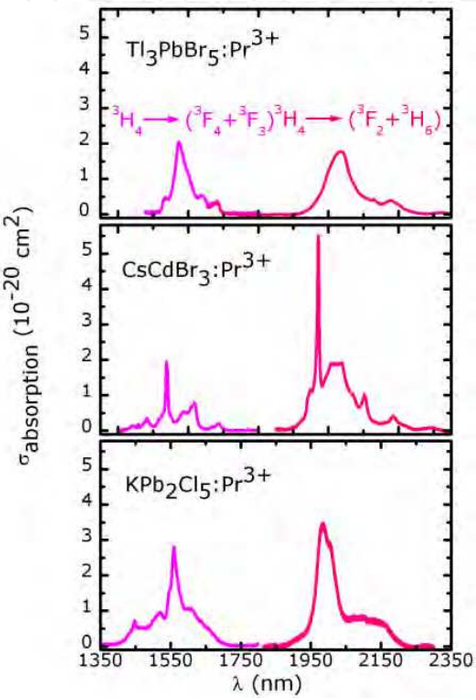

Fig. 8. Absorption cross sections around 1.55 and 2 µm at room temperature. The absorption cross section around 4.6 µm are shown in figure 10.

Judd-Ofelt analysis realized with absorption spectra on the 10 first excited states, among which 3 of them ($^3F_2$, $^3F_4$ and $^1I_6$) were thermalized with their closest lower lying level, showed that the branching ratio of the ($^3F_4$,$^3F_3$)→$^3F_2$ transition is negligibly small, that of the ($^3F_4$,$^3F_3$)→$^3H_6$ transition amounts to ~2.3 % (resp. ~1.6 %) and that the radiative lifetime of ($^3F_4$,$^3F_3$) levels is ~0.5 ms (resp. ~1 ms) in KPb_2Cl_5 (resp. $CsCdBr_3$) (for experimental lifetimes of ~0.096 ms in KPb_2Cl_5, ~1.57 ms in $CsCdBr_3$ and ~0.89 ms in Tl_3PbBr_5). Despite similarly weak branching ratios in $LaCl_3$ crystals, laser operations at 5.2 and 7.2 µm could be evidenced [Bowman et al., 1994, 1996]. Utilizing a flash lamp pumped phosphate glass Kigre laser at 1.54 µm, delivering pulse trains of 30 mJ at a frequency of 2 to 10 Hz, no luminescence issued from ($^3F_4$,$^3F_3$) multiplets at these two wavelengths could be observed in KPb_2Cl_5, $CsCdBr_3$ and Tl_3PbBr_5 crystals. However, luminescence at 1.6 and 2.4 µm associated to ($^3F_4$,$^3F_3$)→$^3H_4$ (β~74 % in KPb_2Cl_5, ~61.3 % in $CsCdBr_3$) and ($^3F_4$,$^3F_3$)→$^3H_5$ (β~24 % in KPb_2Cl_5, ~37 % in $CsCdBr_3$) transitions were observed (figure 9).

Broad band emission spectra are poorly structured and exhibit important emission cross section, ~(2-4).10^{-20} cm^2 ($\sigma_{EM}\tau_R$~(2-4).10^{-23} cm^2.s at the emission peak, virtually as much as in YAG:Nd^{3+} at 1.064 μm), in the two compounds $CsCdBr_3$ and KPb_2Cl_5. Several levels emit around 4.5-5 μm [Rana & Kaseta, 1983] : the ($^3F_4$,$^3F_3$) levels around 5 μm, the ($^3F_2$,$^3H_6$) levels around 4.5 μm and the $^3H_6$ level around 4.9 μm. The former ones already gave rise to the laser operation described in section 1, but in comparison with the other levels, the branching

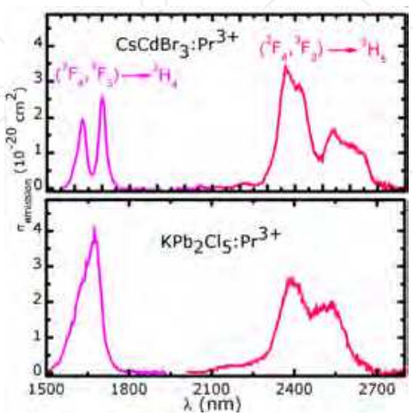

Fig. 9. Room temperature emission spectra of Pr^{3+} ions dissolved into $CsCdBr_3$ and KPb_2Cl_5 crystals, excited by pulses of a Kigre Er^{3+} laser at 1.54 μm.

ratio of the laser transition proves to be rather weak (~2.3 % (resp. ~1.6 %) versus ~14.7 % (resp. ~8.4 %) and ~48.4 % (resp. ~54.4%) in KPb_2Cl_5 (resp. $CsCdBr_3$)). The $^3H_6 \rightarrow {}^3H_5$ transition seems interesting not only because of its branching ratio, but also because the experimental lifetime is quite long, 1 ms (3.6 ms in $CsCdBr_3$), and so favourable to energy storage. Nevertheless, this transition competes with ground state absorption and energy transfer processes induced by the excitation at 2 μm, likely to provoke important losses. Finally, the simplest solution remains the $^3H_5 \rightarrow {}^3H_4$ transition which, even if it ends on the ground state, has a long lifetime, a quantum yield close to 1 (β=100 %) and broad and high absorption and emission cross sections. Such an emission could be efficiently pumped by means of QCL diodes around 4.6 μm. Although several energy levels (($^3F_4$,$^3F_3$), ($^3F_2$,$^3H_6$) and $^3H_6$) can emit around 4-5 μm, by means of the same excitation scheme as described above, and with a time resolved detection, it was possible to discriminate the IR luminescence associated with the $^3H_5 \rightarrow {}^3H_4$ transition, and to calibrate the spectra in cross section units by means of the Fuchtbauer-Ladenburg formula (for Tl_3PbBr_5, we took the experimental lifetime, $\tau_f(^3H_5)$=30 ms). Absorption and emission spectra around 4.6 μm turn out to be very broad in the three compounds (figure 10). The emission cross section is about twice that found in KPb_2Cl_5:Er^{3+} around 4.5 μm and the radiative lifetimes are several tens of ms ($\sigma_{EM}\tau_R$~(2-3).10^{-22} cm^2.s at the peak). Judd-Ofelt analysis gives $\tau_R(^3H_5)$=38 ms (versus τ_f=5.65 ms in KPb_2Cl_5), $\tau_R(^3H_5)$=82 ms (versus τ_f=29 ms dans $CsCdBr_3$), once again favourable to energy storage with a view to short-pulse MIR laser operation. For a total Pr^{3+} ions concentration typically ~10^{20} (resp. 5.10^{19}) cm^{-3} and a crystal length of 5 mm, the absorption rate of a pump beam at 4.6 μm would reach 21.3 (resp. 11.3) %. The emission lines profiles, shown in figure 10 for the two compounds KPb_2Cl_5 and $CsCdBr_3$, were checked by calibrating them by the reciprocity method, and the agreement with the previous spectra is

satisfying [Ferrier et al., 2008b, 2009b]. Gain cross section calculated with these spectra are displayed in figure 11. In the case of KPb_2Cl_5 and of Tl_3PbBr_5, the gain cross section is very broad and devoid of maximum, which could give rise to a broad tunability over a large spectral range. In the case of $CsCdBr_3$, the gain cross section, weaker, exhibits a peak at 4.75 µm and a rounded shape ~5 µm, where laser operation is expected. In all cases, we observe that the gain cross section is positive as soon as ζ=0.4, from 4.96 to 5.6 µm for $CsCdBr_3$, and from 4.87 to 5.48 µm for KPb_2Cl_5. As this type of 3-level lasers require a high population inversion ratio (ζ=0.4), an efficient pumping source must be designed, which can excite the strongest absorption bands around 1.6 ($^3H_4 \rightarrow (^3F_4, ^3F_3)$) and 2 µm ($^3H_4 \rightarrow (^3F_2, ^3H_6)$) with solid state lasers or Er^{3+} or Tm^{3+}-doped fibers now widely spread.

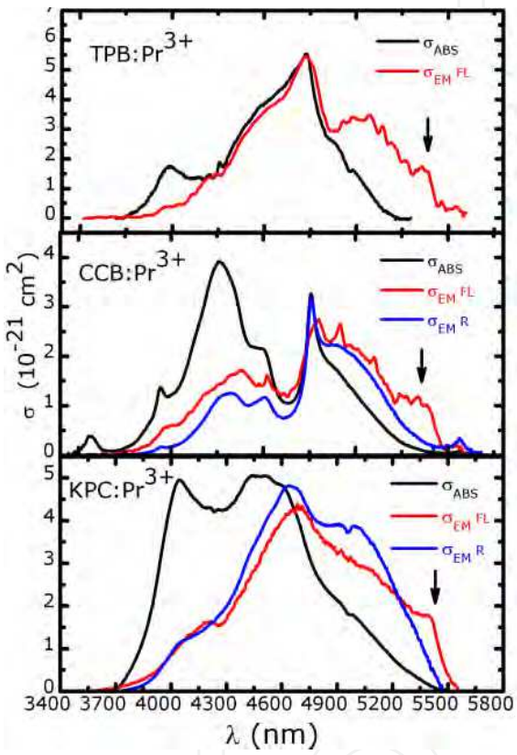

Fig. 10. Absorption and emission cross sections between $^3H_5$ and $^3H_4$ levels at room temperature. The arrow indicates an artefact peak due to the response function of a filter λ>3.5 µm incorporated in the setup in order to eliminate fluorescence harmonics.

Another way would consist in codoping the crystal with Yb^{3+} ions (resp. Tm^{3+} ions), and to exploit Yb^{3+}-Pr^{3+} energy transfer [Balda et al., 2003; Bluiett et al., 2008; Howse et al., 2010] thanks to high-powered low cost 980 nm (resp. 800 nm) diode pumping, but the high concentrations required remain hardly achievable in these compounds on the one hand, and the energy difference between laser and pumping wavelengths which would entail an important thermal load, on the other hand, lead us to consider another promising alternative : QCL diode pumping around 4.6 µm (which delivers 1.8 W at room temperature [Bai et al., 2008]), that is, pumping directly in the emitting level. Preliminary calculations, which do not take into account neither excited state absorption nor energy transfers, suggest that these sources should allow for reaching a sufficient population inversion ratio to obtain

laser operation at reasonable pumping powers with power conversion yields on the order ~10 % [Ferrier et al., 2008b, 2009b].

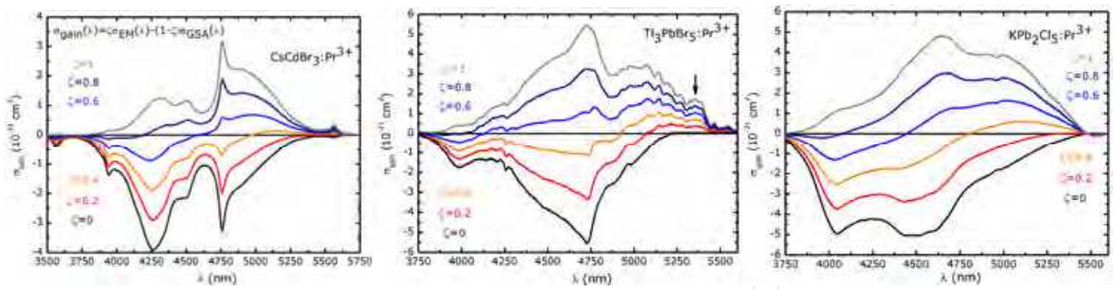

Fig. 11. Effective gain cross section around 4-5 μm in $CsCdBr_3$, Tl_3PbBr_5 and KPb_2Cl_5 doped with Pr^{3+}, with $\zeta = n^3H_5/(n^3H_5+n^3H_4)$.

Let us stress once again the necessity of both obtaining microstructure-related loss-free crystals and designing an efficient pumping scheme. Indeed, even if the gain cross section becomes positive at 40 % population inversion, the latter quickly saturates at 53.5 % in $KPb_2Cl_5:Pr^{3+}$ for a pump beam waist at 4.6 μm of 100 μm, and one expects laser emission centered at 5.05 μm, where the gain cross section reaches a low $\sim 1.1\times10^{-21}$ cm^2 (figure 11). For a crystal length of 5 mm and an excited ion concentration of 10^{19} cm^{-3}, the cavity roundtrip gain amounts to 1.1 %, that is, virtually the same as that found in $KPb_2Cl_5:Er^{3+}$. In order to explain the homogeneous and inhomogeneous substantial broadening of the absorption and emission bands in $Pr^{3+}:KPb_2Cl_5$, a scrutinous examination of the absorption line profile on the $^3P_0$ profile at 487.5 nm is mandatory [Ferrier et al., 2008b]. As a matter of fact, for this non degenerate level one expects one single line per substitution site, provided that the second crystal field sublevel of the ground state $^3H_4$ does not contribute to the absorption signal shape : as it lies at 15 cm^{-1}, it should not be significantly populated at temperatures lower than 21.6 K. Figure 12 clearly shows the presence of five absorption lines and consequently as many substitution sites for Pr^{3+} ions in KPb_2Cl_5, giving a beginning of explanation to the origin of the inhomogeneous band broadening, which consequently dominates the homogeneous broadening at low temperature [Ferrier et al., 2008b].

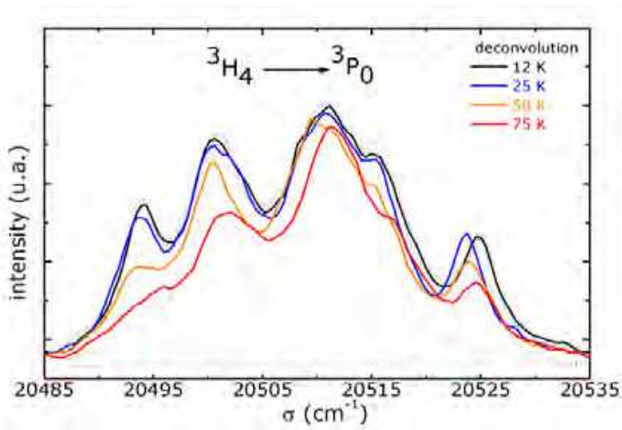

Fig. 12. Ground state absorption on the $^3P_0$ level of Pr^{3+} ions dissolved into KPb_2Cl_5, at low temperature and as a function of temperature. Five lorentzian functions are necessary to deconvolute the whole signal.

This characteristic is consistent with the structural description of the point defects [Velázquez et al., 2006b], but if it is so, why does Er^{3+} or Eu^{3+} substitution lead to majoritarily one type of point defect [Cascales et al., 2005; Ferrier et al., 2007; Gruber et al., 2006; Velázquez et al., 2009] ? Moreover this characteristic confirms the advantage of using KPb_2Cl_5 instead of $LaCl_3$, the lines of which are much narrower and force the experimentalist to find a pumping source emitting precisely, for instance, at 1.54 µm. Fluorescence around 1.6 and 2.4 µm, associated with $(^3F_4,^3F_3)\rightarrow{}^3H_4$ and $(^3F_4,^3F_3)\rightarrow{}^3H_5$ transitions obtained under excitation at 2.012 µm with a YAG:Tm^{3+}, give strong evidence for efficient energy transfers from the $(^3F_2,^3H_6)$ levels.

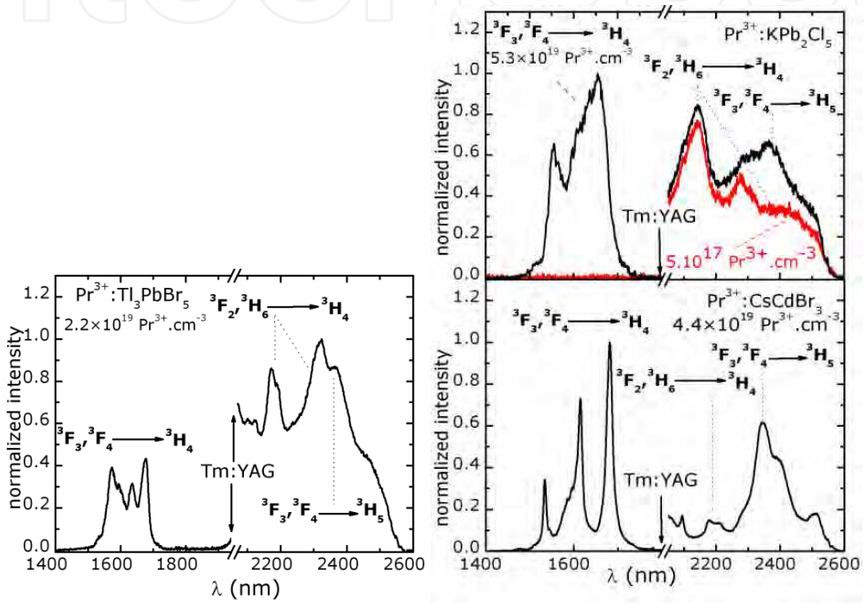

Fig. 13. Emission spectra, recorded at room temperature, under cw excitation at 2.011 µm (YAG:Tm), issued from $(^3F_4,^3F_3)$ and $(^3F_2,^3H_6)$ levels.

In Figure 13, we see that these energy transfers do not only occur undistinctly in KPb_2Cl_5 and in $CsCdBr_3$, but that they also occur in the former compound with Pr^{3+} ions concentrations a hundred times weaker. The Pr^{3+} ion pairing in $CsCdBr_3$, favourable to energy transfers described above, can be related to the decrease by a factor of 4 of the relative intensity of the emission issued from $(^3F_2,^3H_6)$ levels in favour of those issued from $(^3F_4,^3F_3)$ levels.

Finally, another alternative could be found in the works performed on Tb^{3+} and (Tb^{3+},Tm^{3+})-doped KPb_2Cl_5, KPb_2Br_5 and $CsCdBr_3$ single crystals, because of their potentially interesting MIR transitions $^7F_5\rightarrow{}^7F_6$ (4.6-5.5 µm) and $^7F_4\rightarrow{}^7F_5$ (8 µm) [Bluiett et al., 2011; Ganem et al., 2002; Lichkova et al., 2006; Okhrimchuk et al., 2002; Rademaker et al., 2004; Roy et al., 2005; Shakurov et al., 2004]. So far, no laser operation based on these systems could be demonstrated. The $^7F_6$ multiplet is both the terminal level and ground state and the branching ratio of the $^7F_4\rightarrow{}^7F_5$ transition is ~2 % (resp. ~6.6 %) and the experimental lifetimes of several tens of ms (resp. $\tau(^7F_5)\approx22$ ms and $\tau(^7F_4)\approx0.36$ ms) in KPb_2Cl_5 (resp. KPb_2Br_5 [Hömmerich et al., 2006]).

4. Loss mechanisms and current challenges in the growth of MIR laser halide crystals

The growth conditions of pure or RE^{3+}-doped APb_2X_5 (A=K,Rb ; X=Cl,Br) and Tl_3PbX_5 (X=Cl,Br) single crystals for MIR laser and/or nonlinear optical applications have been exhaustively detailed in an impressive body of work [Amedzake et al., 2008; Atuchin et al., 2011; Bekenev et al., 2011; Condon et al., 2006b; Ferrier et al., 2006a, 2006b; Gang et al., 2008; Isaenko et al., 2001; Nitsch et al., 1993, 1995a, 1995b, 2004; Nitsch & Rodová 1999; Oyebola et al., 2010; Rodová et al., 1995; Roy et al., 2003; Singh et al., 2005; Tigréat et al., 2001; Velázquez et al., 2006a, 2006b, 2009; Voda et al., 2004; Wang et al., 2007]. Special safety conditions for the manipulation of large amounts of TlCl or TlBr powders must be followed, but this does not entail insuperable difficulties [Peter & Viraraghavan, 2005]. It is now widely established that crystal growth by the Bridgman method must be carried out in sealed silica ampoules under a low pressure (~10^{-2} atm) of Cl_2 or HCl (HBr for bromides) gas to avoid bubble formation, and at low growth rates (~0.1-1 $mm.h^{-1}$) in axial thermal gradients typically 15-20 $K.cm^{-1}$ with opening angles of the ampoule bottom lower than 120° to avoid shear stress induced cracks. PbX_2 (X=Cl,Br) starting materials must be purified by previous solidification runs by the Bridgman method [Basiev et al., 2004]. In KPb_2Cl_5 crystals, roundtrip losses mechanisms, such as laser beam depolarization and double refraction [Condon et al., 2006b], are likely to be due to a classical kind of twinning, which occurs above a finite stress threshold, consisting in twin planes perpendicular to [100] and [001] directions and leading to a loss of the laser power transmitted within the cavity of up to 50 %. This has seriously hindered further development of highly brilliant laser systems at 4.6 μm (and presumably higher wavelengths), since with an absorption cross section σ_{abs} ≈2.10^{-21} cm^2 at 800 nm, an Er^{3+} ion concentration $n_{^4I_{15/2}}$ ~5.10^{19} cm^{-3} and a typical crystal length of 5 mm, the pump beam absorption rate in a classical two-mirror cavity based on a KPb_2Cl_5:Er^{3+} amplifier is about 5 %. On the other hand, the expected round-trip gain ($g = 2\sigma_{ém} n_{^4I_{9/2}} \ell$, for a 100 % inversion rate), in an otherwise perfect crystal unaffected by thermal lens nor birefringence effects, with $n_{^4I_{9/2}}$ ~5.10^{18} cm^{-3} and $\sigma_{em}(4.53\mu m) \approx 1.9\times10^{-21}$ cm^2, barely reaches 1 %. So, the two main current challenges in terms of laser crystal growth are to increase the Er^{3+} ion content and avoid twinning of the crystals upon cooling. The twinning patterns observed under polarized light are due to the phase transition that occurs upon cooling the crystal, at T_t=255 °C. The mechanism of this phase transition has been definitely unveiled in recent years simultaneously by us and a Russian team [Mel'nikova et al., 2005, 2006; Merkulov et al., 2005; Velázquez et al., 2006b, 2009; Velázquez & Pérez, 2007]. The phase transition is driven by the K^+ and $Pb(2)^{2+}$ cationic ordering that induces a Pmcn to $P2_1/c$ symmetry change upon cooling, at 255 °C. Similar twinning patterns were observed in KPb_2Br_5 crystals [Mel'nikova et al., 2005], and twinning patterns associated with the crossing of another phase transition was also observed in Tl_3PbBr_5 [Singh et al., 2005]. It is possible to produce, by means of slow cooling, small size (~1 to 8 mm^3) untwined single crystals, but any stress of magnitude higher than a certain threshold value will result in the formation of a twinning pattern. In order to get rid of that, one must increase the diffusion activation energy, E_a, by increasing the radius of the A^+ cation in APb_2X_5 (X=Cl,Br) compounds, in such a way that $E_a > RT_m$, with T_m=432.3 °C for KPb_2Cl_5. On passing from A=K to A=Rb, the crystal does

not undergo any phase transition between the melting and room temperatures, which explains the interest of several research groups in developing RE-doped $RbPb_2Cl_5$ crystals. However, according to our preliminary experiments, in rubidium lead chloride crystals, the Er^{3+} solubility seems lower than in potassium lead chlorides. So, it is clear that some innovative codoping of Er^{3+} ions with another ion devoid of optical activity must be found, in order to increase its solubility in rubidium lead halides [Isaenko et al., 2009b; Tarasova et al., 2011; Velázquez et al., 2009].

5. Conclusion

This chapter has emphasized the laser potential of the currently most important rare-earth doped chlorides and bromides laser crystals. Some of them ($LaCl_3:Pr^{3+}$, $KPb_2Cl_5:Er^{3+}$, $KPb_2Cl_5:Dy^{3+}$) have already led to laser systems operating in bands II and III of the atmosphere transmission window. All these crystals were grown exclusively by the Bridgman method in sealed silica ampoules. After 15 years of research on MIR solid state lasers carried out in Europe, USA, Russia and more recently China, lots of improvements remain to be done in the realm of synthesis and crystal growth of the laser materials, as well as on the optimization of the pumping strategy. Both kind of advances will require new and original solid solution crystal engineering in order to both get rid of the phase transition inducing twinned microstructures detrimental to efficient laser operation and increase the suitable RE ions solubilities in the halide host compounds. As the gain cross sections in the spectral range where laser operation was demonstrated are relatively weak (~(1-5).10^{-21} cm^2), an important effort must be devoted to the annihilation of the losses which could also be achieved by a clever shaping and functionalization of the crystals. In this perspective, 3-level laser operation by QCL diode pumping on the Pr^{3+} $^3H_5$ multiplet in KPb_2Cl_5 crystals could be interesting because of the low thermal load, the substantial absorption cross section and also because the refractive index difference between twin domains should be much smaller in this spectral range.

6. References

Aleksandrov, K. S.; Vtyurin, A. N.; Eliseev, A. P.; Zamkova, N. G.; Isaenko, L. I.; Krylova, S.N.; Pashkov, V. M.; Turchin, P. P. & Shebanin, A. P. (2005). Vibrational spectrum and elastic properties of KPb_2Cl_5 crystals. *Phys. Sol. St.*, Vol. 47, No.3, pp. 531-538.

Amedzake, P.; Brown, E.; Hömmerich, U.; Trivedi, S. B. & Zavada, J. M. (2008). Crystal growth and spectroscopic characterization of Pr-doped KPb_2Cl_5 for mid-infrared laser applications. *J. Cryst. Growth*, Vol. 310, pp. 2015-2019.

An, Y. & May, P. S. (2006). Temperature dependence of excited-state relaxation processes of Pr^{3+} in Pr-doped and Pr,Gd-doped $CsCdBr_3$. *J. Lum.*, Vol. 118, pp. 147-157.

Atuchin, V. V.; Isaenko, L. I.; Kesler, V. G. & Tarasova, A. Yu. (2011). Single crystal growth and surface chemical stability of KPb_2Br_5. *J. Cryst. Growth*, Vol. 318, No.1, pp. 1000-1004.

Bai, Y.; Slivken, S.; Davish, S. R. & Razeghi, M. (2008). Room temperature continuous wave operation of quantum cascade lasers with 12.5% wall plug efficiency. *Appl. Phys. Lett.*, Vol. 93, No.2, pp. 021103/1-3.

Balda, R.; Voda, M.; Al-Saleh, M. & Fernandez, J. (2002). Visible luminescence in $KPb_2Cl_5:Pr^{3+}$ crystal. *J. Lumin.*, Vol. 97, pp. 190-197.

Balda, R.; Fernández, J.; Mendioroz, A.; Voda, M. & Al-Saleh, M. (2003). Infrared-to-visible upconversion processes in Pr^{3+}/Yb^{3+}-codoped KPb_2Cl_5. *Phys. Rev. B*, Vol. 68, pp. 165101/1-7.

Balda, R.; Garcia–Adeva, A. J.; Voda, M. & Fernández, J. (2004). Upconversion processes in Er^{3+}-doped KPb_2Cl_5. *Phys. Rev. B*, Vol. 69, pp. 205203/1-8.

Basiev, T. T. ; Danileiko, Yu. K.; Dmitruk, L. N.; Galagan, B. I.; Moiseeva, L. V.; Osiko, V. V.; Sviridova, E. E. & Vinogradova, N. N. (2004). The purification, crystal growth, and spectral-luminescent properties of $PbCl_2$:RE. *Opt. Mater.*, Vol. 25, pp. 295-299.

Bekenev, V. L.; Khyzhun, O. Yu.; Sinelnichenko, A. K.; Atuchin, V. V.; Parasyuk, O. V.; Yurchenko, O. M.; Bezsmolnyy, Yu.; Kityk, A. V.; Szkutnik, J. & Calus, S. (2011). Crystal growth and the electronic structure of Tl_3PbCl_5. *J. Phys. Chem. Sol.*, Vol. 72, No.6, pp. 705-713.

Bluiett, A. G.; Pinkney, E.; Brown, E. E.; Hömmerich, U.; Amedzake, P.; Trivedi, S. B. & Zavada, J. M. (2008). Energy transfer processes in doubly doped Yb,Pr:KPb_2Cl_5 for mid-infrared laser applications. *Mater. Sci. Engin. B*, Vol. 146, pp. 110-113.

Bluiett, A. G.; Peele, D.; Norman, K.; Brown, E.; Hömmerich, U.; Trivedi, S. B. & Zavada, J. M. (2011). Mid-infrared emission characteristics and energy transfer processes in doubly doped Tm,Tb:KPb_2Br_5 and Tm,Nd:KPb_2Br_5. *Opt. Mater.*, Vol. 33, pp. 985-988.

Bowman, S. R.; Ganem, J.; Feldman, B. J. & Kueney, A. W. (1994). Infrared laser characteristics of praseodymium-doped lanthanum trichloride. *IEEE J. Quant. Elect.*, Vol. 30, No.12, pp. 2925-2928.

Bowman, S. R.; Shaw, L. B.; Feldman, B. J. & Ganem, J. (1996). A 7-μm praseodymium-based solid-state laser. *IEEE J. Quant. Elect.*, Vol. 32, No.4, pp. 646-649.

Bowman, S. R.; Searles, S. K.; Ganem, J. & Smidt, P. (1999). Further investigations of potential 4-μm laser materials. *Trends in Optics and Photonics*; Fejer, M. M., Ingeyan, H., Keller, U., Eds.; Optical Society of America : Washington, DC, Vol. 26, pp. 487-490.

Bowman, S. R.; Searles, S. K.; Jenkins, N. W.; Qadri, S. B. & Skelton, E. F. (2001). Diode pumped room temperature mid-infrared erbium laser. *Trends in Optics and Photonics*; Marshall, C. Ed.; Optical Society of America : Washington, DC, Vol. 50, pp. 154-156.

Cascales, C.; Fernández, J. & Balda, R. (2005). Investigation of site-selective symmetries of Eu^{3+} ions in KPb_2Cl_5 by using optical spectroscopy. *Optics Express*, Vol. 13, No.6, pp. 2141-2152.

Chukalina, E. P. (2004). Study of hyperfine structure in the optical spectra of crystals doped with Pr^{3+} and Er^{3+} ions. *J. Opt. Techn.*, Vol. 71, No.9, pp. 581-585.

Cockroft, N. J.; Jones, G. D. & Nguyen, D. C. (1992). Dynamics and spectroscopy of infrared-to-visible upconversion in erbium-doped cesium cadmium bromide ($CsCdBr_3:Er^{3+}$). *Phys. Rev. B*, Vol. 45, No.10, pp. 5187-5198.

Condon, N. J.; O'Connor, S. & Bowman, S. R. (2006a). Growth and mid-infrared laser performance of Er^{3+}:KPb_2Cl_5. *IEEE LEOS Annual Meeting, Conference Proceedings, 19th*, Montreal, QC, Canada, Oct. 29-Nov. 2, Vol. 2, pp. 743-744.

Condon, N. J.; O'Connor, S. & Bowman, S. R. (2006b). Growth and characterization of single-crystal Er^{3+}:KPb_2Cl_5 as a mid-infrared laser material. *J. Crystal Growth*, Vol. 291, pp. 472-478.

Doualan, J.-L. & Moncorgé, R. (2003). Laser crystals with low phonon frequencies. *Ann. Chim. Sci. Mat.*, Vol. 28, pp. 5-20.

Egger, P.; Burkhalter, R. & Hulliger, J. (1999). Czochralski growth of $Ba_2Y_{1-x}Er_xCl_7$ ($0<x\leq1$) using growth equipment integrated into a dry-box. *J. Cryst. Growth*, Vol. 200, pp. 515-520.

Ferrier, A. ; Velázquez, M.; Portier, X. ; Doualan, J.-L. & Moncorgé, R. (2006a). Tl_3PbBr_5 : a possible crystal candidate for middle infrared nonlinear optics. *J. Cryst. Growth*, Vol. 289, No.1, pp. 357-365. Note that in this paper, a misprint error occurred: we used a KDP and not a KD*P powder as a standard.

Ferrier, A.; Velázquez, M.; Pérez, O.; Grebille, D.; Portier, X. & Moncorgé, R. (2006b). Crystal growth and characterization of the non-centrosymmetric compound Tl_3PbCl_5. *J. Cryst. Growth*, Vol. 291, No.2, pp. 375–384.

Ferrier, A.; Velázquez, M.; Doualan, J.-L.; Moncorgé, R. (2007). Energy level structure and excited-state absorption properties of Er^{3+}-doped KPb_2Cl_5. *J. Opt. Soc. Amer. B*, Vol. 24, pp. 2526-2536.

Ferrier, A.; Velázquez, M. & Moncorgé, R. (2008a). Spectroscopic characterization of Er^{3+}-doped Tl_3PbBr_5 for midinfrared applications. *Phys. Rev. B*, Vol. 77, pp. 075122/1-11.

Ferrier, A.; Velázquez, M.; Doualan, J.-L. & Moncorgé, R. (2008b). Midinfrared luminescence properties and laser potentials of Pr^{3+} doped KPb_2Cl_5 and $CsCdBr_3$. *J. of Applied Physics*, Vol. 104, pp. 123513.

Ferrier, A.; Velázquez, M.; Doualan, J.-L. & Moncorgé, R. (2009a). Pr^{3+}-doped Tl_3PbBr_5 : a non hygroscopic, non-linear and low-energy phonon single crystal for the mid-infrared laser application. *Appl. Phys. B*, Vol. 95, pp. 287-291.

Ferrier, A.; Velázquez, M.; Doualan, J.-L. & Moncorgé, R. (2009b). Spectroscopic investigation and mid-infrared luminescence properties of the Pr^{3+} doped low phonon single crystals $CsCdBr_3$, KPb_2Cl_5 and Tl_3PbBr_5. *J. Lumin.*, Vol. 129, No.12, pp. 1905-1907.

Gafurov, M. R.; Iskhakova, A. I.; Kurzin, I. N.; Kurzin, S. P.; Malkin, B. Z.; Nikitin, S. I.; Orlinskii, S. B.; Rakhmatullin, R. M.; Shakurov, G. S.; Tarasov, V. F.; Demirbilek, R. & Heber, J. (2002). Spectra and relaxation of electronic excitations in $CsCdBr_3$:Yb^{3+} and $CsCdBr_3$:Nd^{3+} single crystals. *SPIE Proceedings*, Vol. 4766, pp. 279-291.

Ganem, J.; Crawford, J.; Schmidt, P.; Jenkins, N. W. & Bowman, S. R. (2002). Thulium cross-relaxation in a low phonon energy crystalline host. *Phys. Rev. B*, Vol. 66, pp. 245101/1-15.

Gang, C.; Chun-he, Y.; Jian-rong, C.; Hai-li, W. & Nan-hao, Z. (2008). *Rengong Jingti Xuebao*, Vol. 37, No.6, pp. 1567-1570.

Guillot-Noël, O.; Goldner, P.; Higel, P. & Gourier, D. (2004). A practical analysis of electron paramagnetic resonance spectra of rare earth ion pairs. *J. Phys. : Condens. Matter*, Vol. 16, pp. R1-R24.

Gruber, J. B.; Yow, R. M.; Nijjar, A. S.; Russell, C. C.; Sardar, D. K.; Zandi, B.; Burger, A. & Roy, U. N. (2006). Modeling the crystal-field splitting of energy levels of Er^{3+} ($4f^{11}$) in charge-compensated sites of KPb_2Cl_5. *J. Appl. Phys.*, Vol. 100, pp. 0431081-6.

Heber, J.; Demirbilek, R.; Altwein, M.; Kübler, J.; Bleeker, B. & Meijerink, A. (2001). Electronic states and interactions in pure and rare-earth doped $CsCdBr_3$. *Radiation Effects & Defects in Solids*, Vol. 154, pp. 223-229.

Hömmerich, U.; Nyein, E. E. & Trivedi, S. B. (2005). Crystal growth, upconversion, and infrared emission properties of Er^{3+}-doped KPb_2Br_5. *J. Lum.*, Vol. 113, pp. 100-108.

Hömmerich, U.; Brown, E.; Amedzake, P.; Trivedi, S. B. & Zavada, J. M. (2006). Mid-infrared (4.6 μm) emission properties of Pr^{3+} doped KPb_2Br_5. *J. Appl. Phys.*, Vol. 100, pp. 113507/1-4.

Howse, D.; Logie, M.; Bluiett, A. G.; O'Connor, S.; Condon, N. J.; Ganem, J. & Bowman, S. R. (2010). Optically-pumped mid-IR phosphor using Tm^{3+}-sensitized Pr^{3+}-doped KPb_2Cl_5. *J. Opt. Soc. Am. B*, Vol. 27, No.11, pp. 2384-2392.

Isaenko, L.; Yelisseyev, A.; Tkachuk, A.; Ivanova, S.; Vatnik, S.; Merkulov, A.; Payne, S.; Page, R. & Nostrand, M. (2001). New laser crystals based on KPb_2Cl_5 for IR region. *Mater. Sci. Eng. B*, Vol. 81, pp. 188-190.

Isaenko, L.; Yelisseyev, A.; Tkachuk, A. & Ivanova, S. (2008). New monocrystals with low phonon energy for mid-IR lasers. In *Mid-Infrared Coherent Sources and Applications*; Ebrahim-Zadeh, M., Sorokina, I. T., Eds.; Springer : New York, pp. 3-65.

Isaenko, L. I.; Merkulov, A. A.; Tarasova, A. Yu.; Pashkov, V. M. & Drebushchak, V. A. (2009a). Coefficients of thermal expansion of the potassium and rubidium halogenide plumbates. *J. Therm. Anal. Cal.*, Vol. 95, No.1, pp. 323-325.

Isaenko, L. I.; Mel'nikova, S. V.; Merkulov, A. A.; Pashkov, V. M. & Tarasova, A. Yu. (2009b). Investigation of the influence of gradual substitution K/Rb on the structure and phase transition in $K_xRb_{1-x}Pb_2Br_5$ solid solutions. *Physics of the Solid State*, Vol. 51, No.3, pp. 589-592.

Jenkins, N. W.; Bowman, S. R.; O'Connor, S.; Searles, S. K. & Ganem, J. (2003). Spectroscopic characterization of Er-doped KPb_2Cl_5 laser crystals. *Opt. Mater.*, Vol. 22, pp. 311-320.

John Peter, A. L. & Viraraghavan, T. (2005). Thallium : a review of public health and environmental concerns. *Environment International*, Vol. 31, pp. 493-501.

Kaminska, A.; Cybińska, J.; Zhydachevskii, Ya.; Sybilski, P.; Meyer, G. & Suchocki, A. (2011). Luminescent properties of ytterbium-doped ternary lanthanum chloride. *J. All. Comp.*, Vol. 509, pp. 7993-7997.

Lichkova, N. V.; Zagorodnev, V. N.; Butvina, L. N.; Okhrimchuk, A. G. & Shestakov, A. V. (2006). Preparation and optical properties of rare-earth-activated alkali metal lead chlorides. *Inorg. Mater.*, Vol. 42, No.1, pp. 81-88.

Malkin, B. Z.; Iskhakova, A. I.; Kamba, S.; Heber, J.; Altwein, M. & Schaak, G. (2001). Far-infrared spectroscopy investigation and lattice dynamics simulations in $CsCdBr_3$ and $CsCdBr_3$:R^{3+} crystals. *Phys. Rev. B*, Vol. 63, pp. 075104-1/11.

Mel'nikova, S. V.; Isaenko, L. I.; Pashkov, V. M. & Pevnev, I. V. (2005). Phase transition in a KPb_2Br_5 crystal. *Phys. Sol. St.*, Vol. 47, No.2, pp. 332-336.

Mel'nikova, S. V.; Isaenko, L. I.; Pashkov, V. M. & Pevnev, I. V. (2006). Search for and study of phase transitions in some representatives of the APb_2X_5 family. *Phys. Sol. St.*, Vol. 48, No.11, pp. 2152-2156.

Merkulov, A. A.; Isaenko, L. I.; Pashkov, V. M.; Mazur, V. G.; Virovets, A. V. & Naumov, D. Yu. (2005). Crystal structure of KPb_2Cl_5 and KPb_2Br_5. *J. Struct. Chem.*, Vol. 46, No.1, pp. 103-108.

Neukum, J.; Bodenschatz, N. & Heber, J. (1994). Spectroscopy and upconversion of $CsCdBr_3$:Pr^{3+}. *Phys. Rev. B*, Vol. 50, No.6, pp. 3536-3546.

Nitsch, K.; Cihlář, A.; Malková, Z.; Rodová, M.; Vaněček, M. (1993). The purification and preparation of high-purity lead chloride and ternary alkali lead chloride single crystals. *J. Crystal Growth*, Vol. 131, pp. 612.

Nitsch, K.; Dušek, M.; Nikl, M.; Polák, K.; Rodová, M. (1995a). Ternary alkali lead chlorides : crystal growth, crystal structure, absorption and emission properties. *Prog. Cryst. Growth Charact.*, Vol. 30, pp. 1–22.

Nitsch, K.; Cihlář, A.; Nikl, M.; Rodová, M. (1995b). Growth of lead bromide and ternary alkalic lead bromide single crystals. *J. Electr. Eng.*, Vol. 46, No.8/s, pp. 82-84.

Nitsch, K. & Rodová, M. (1999). Influence of thermal treatment on supercooling of molten potassium lead chloride. *J. Elect. Eng.*, Vol. 50, No.2/s, pp. 35-37.

Nitsch, K.; Cihlář, A. & Rodová, M. (2004). Molten state and supercooling of lead halides. *J. Cryst. Growth*, Vol. 264, pp. 492–498.

Nostrand, M. C.; Page, R. H.; Payne, S. A.; Krupke, W. F.; Schunemann, P. G. & Isaenko, L. I. (1998). Spectroscopic data for infrared transitions in $CaGa_2S_4$:Dy^{3+} and KPb_2Cl_5:Dy^{3+}. *Trends in Optics and Photonics*; Bosenberg, W. R. and Fejer, M. M., Eds.; Optical Society of America : Washington, DC; Vol. 19, pp. 524-528.

Nostrand, M. C.; Page, R. H.; Payne, S. A.; Krupke, W. F.; Schunemann, P. G. & Isaenko, L. I. (1999). Room temperature $CaGa_2S_4$:Dy^{3+} laser action at 2.43 and 4.31 μm and KPb_2Cl_5:Dy^{3+} laser action at 2.43 μm. *Trends in Optics and Photonics*; Fejer, M. M.,

Ingeyan, H., Keller, U., Eds.; Optical Society of America : Washington, DC; Vol. 26, pp. 441-449.

Nostrand, M. C.; Page, R. H.; Payne, S. A.; Isaenko, L. I. & Yelisseyev, A. P. (2001). Optical properties of Dy^{3+}- and Nd^{3+}-doped KPb_2Cl_5. *J. Opt. Soc. Am. B*, Vol. 18, No.3, pp. 264–276.

Okhrimchuk, A.; Butvina, L. & Dianov, E. (2002). Sensitization of MIR Tb^{3+} luminescence by Tm^{3+} ions in $CsCdBr_3$ and KPb_2Cl_5 crystals. *Advanced Solid-State Photonics (ASSP)*; OSA Technical Digest Series; paper WB5-1, pp. 273-275.

Okhrimchuk, A. G.; Butvina, L. N.; Dianov, E. M.; Lichkova, N. V.; Zagorodnev, V. N. & Shestakov, A. V. (2006). New laser transition in a Pr^{3+}:$RbPb_2Cl_5$ crystal in the 2.3-2.5-μm range. *Quantum Electronics*, Vol. 36, No.1, pp. 41-44.

Okhrimchuk, A. G.; Butvina, L. N.; Dianov, E. M.; Shestakova, I. A.; Lichkova, N. V.; Zagorodnev, V. N. & Shestakov, A. V. (2007). Optical spectroscopy of the $RbPb_2Cl_5$:Dy3+ laser crystal and oscillation at 5.5 μm at room temperature. *J. Opt. Soc. Am. B*, Vol. 24, No.10, pp. 2690-2695.

Okhrimchuk, A. G. (2008). Dy^{3+} and Pr^{3+} doped crystals for mid-IR lasers. *Conference on Lasers and Electro-Optics & Quantum Electronic and Laser Science Conference*, Vol. 1-9, pp. 1531-1532.

Oyebola, O.; Hömmerich, U.; Brown, E.; Trivedi, S. B.; Bluiett, A. G. & Zavada, J. M. (2010). Growth and optical spectroscopy of Ho-doped KPb_2Cl_5 for infrared solid state lasers. *J. Cryst. Growth*, Vol. 312, No.8, pp. 1154-1156.

Popova, M. N.; Chukalina, E. P.; Malkin, B. Z.; Iskhakova, A. I.; Antic-Fidancev, E.; Porcher P. & Chaminade, J.-P. (2001). High-resolution infrared absorption spectra, crystal field levels, and relaxation processes in $CsCdBr_3$:Pr^{3+}. *Phys. Rev. B*, Vol. 63, pp. 075103-1/10.

Quagliano, J. R.; Cockroft, N. J.; Gunde, K. E. & Richardson, F. S. (1996). Optical characterization and electronic energy-level structure of Er^{3+}-doped $CsCdBr_3$. *J. Chem. Phys.*, Vol. 105, No.22, pp. 9812-9822.

Quimby, R. S.; Condon, N. J.; O'Connor, S. P.; Biswal, S. & Bowman, S. R. (2008). Upconversion and excited-state absorption in the lower levels of Er:KPb_2Cl_5. *Opt. Mater.*, Vol. 30, pp. 827-834.

Rademaker, K.; Krupke, W. F.; Page, R. H.; Payne, S. A.; Petermann, K.; Huber, G.; Yelisseyev, A. P.; Isaenko, L. I.; Roy, U. N.; Burger, A.; Mandal, K. C. & Nitsch, K. (2004). Optical properties of Nd^{3+}- and Tb^{3+}-doped KPb_2Br_5 and $RbPb_2Br_5$ with low nonradiative decay. *J. Opt. Soc. Am. B*, Vol. 21, No.12, pp. 2117-2129.

Rana, R. S. & Kaseta, F. W. (1983). Laser excited fluorescence and infrared absorption spectra of Pr^{3+}:$LaCl_3$. *J. Chem. Phys.*, Vol. 79, No.11, pp. 5280-5285.

Ren, P.; Qin, J. & Chen, C. (2003). A novel nonlinear optical crystal for the IR region : noncentrosymmetrically crystalline $CsCdBr_3$ and its properties. *Inorg. Chem.*, Vol. 42, No.1, pp. 8-10.

Riedener, T.; Egger, P.; Hulliger, J. & Güdel, H. U. (1997). Upconversion mechanisms in Er^{3+}-doped Ba_2YCl_7. *Phys. Rev. B*, Vol. 56, No.4, pp. 1800-1808.

Riedener, T. & Güdel, H. U. (1997). NIR-to-VIS upconversion of Er^{3+} in host materials with low-energy phonons. *Chimia*, Vol. 51, No.3, pp. 95-96.

Rodová, M.; Málková, Z. & Nitsch, K. (1995). Study of hygroscopicity and water-sensitivity of lead halides. *J. Electr. Eng.*, Vol. 46, No.8/s, pp. 79-81.

Roy, U. N.; Cui, Y.; Guo, M.; Groza, M.; Burger, A.; Wagner, G. J.; Carrig, T. J. & Payne, S. A. (2003). Growth and characterization of Er-doped KPb_2Cl_5 as laser host crystal. *J. Cryst. Growth*, Vol. 258, pp. 331–336.

Roy, U. N.; Hawrami, R. H.; Cui, Y.; Morgan, S.; Burger, A.; Mandal, K. C.; Noblitt, C. C.; Speakman, S. A.; Rademaker, K. & Payne, S. A. (2005). Tb^{3+}-doped KPb_2Br_5 : low-energy phonon mid-infrared laser crystal. *Appl. Phys. Lett.*, Vol. 86, pp. 151911/1-3.

Shakurov, G. S.; Malkin, B. Z.; Zakirov, A. R.; Okhrimchuk, A. G.; Butvina, L. N.; Lichkova, N. V. & Zagorodnev, V. N. (2004). High-frequency EPR of Tb^{3+}-doped KPb_2Cl_5 crystal. *Appl. Magn. Reson.*, Vol. 26, pp. 579-586.

Singh, N. B.; Suhre, D. R.; Green, K.; Fernelius, N. & Hopkins, F. K. (2005). Periodically poled materials for long wavelength infrared (LWIR) NLO applications. *J. Cryst. Growth*, Vol. 274, pp. 132-137.

Tarasova, A. Yu.; Isaenko, L. I.; Kesler, V. G.; Pashkov, V. M.; Yelisseyev, A. P.; Denysyuk, N. M. & Khyzhun, O. Yu. (2011). Electronic structure and fundamental absorption edges of KPb_2Br_5, $K_{0.5}Rb_{0.5}Pb_2Br_5$ and $RbPb_2Br_5$ single crystals. *J. Phys. Chem. Sol.*, submitted.

Tigréat, P.-Y.; Doualan, J.-L.; Moncorgé, R. & Ferrand, B. (2001). Spectroscopic investigation of a 1.55 μm emission band in Dy^{3+}-doped $CsCdBr_3$ and KPb_2Cl_5 single crystals. *J. Lumin.*, Vol. 94-95, pp. 107-111.

Tkachuk, A. M.; Ivanova, S. E.; Isaenko, L. I.; Yelisseyev, A. P.; Pustovarov, V. A.; Joubert, M.-F.; Guyot, Y. & Gapontsev, V. P. (2005). Emission peculiarities of TR^{3+}-doped KPb_2Cl_5 laser crystals under selective direct, upconversion and excitonic/host excitation of impurity centers. *Trends in Optics and Photonics*, Vol. 98, Issue Advanced Solid State Photonics, pp. 69-74.

Tkachuk, A. M.; Ivanova, S. E.; Joubert, M.-F.; Guyot, Y.; Isaenko, L. I. & Gapontsev, V. P. (2007). Upconversion processes in Er^{3+}:KPb_2Cl_5 laser crystals. *J. Lumin.*, Vol. 125, pp. 271-278.

Velázquez, M.; Ferrier, A.; Chaminade, J.-P.; Menaert, B. & Moncorgé, R. (2006a). Growth and thermodynamic characterization of pure and Er-doped KPb_2Cl_5. *J. Cryst. Growth*, Vol. 286, No.2, pp. 324–333. In the Figure 1b caption of this article, the Er^{3+} content was mistakenly reported to amount to 0.35 mol %. It is actually 0.35 wt % ≈ 1.32 mol % ≈ 6.10^{19} ions cm^{-3}, or x ≈ 0.013 in $K_{1-x}(V_K)_xPb_{2-x}Er_xCl_5$.

Velázquez, M.; Ferrier, A.; Pérez, O.; Péchev, S.; Gravereau, P.; Chaminade, J.-P. & Moncorgé, R. (2006b). A cationic order-disorder phase transition in KPb_2Cl_5. *Eur. J. Inorg. Chem.*, Vol. 20, pp. 4168–4178. During the typesetting and publishing processes of this article, a minus sign appeared in the "Structure of rare-earth defects" section, that must be systematically replaced by a plus sign.

Velázquez, M. & Pérez, O. (2007). Comments on "Growth and characterization of single crystal Er^{3+}:KPb_2Cl_5 as a mid-infrared laser material". *J. Cryst. Growth*, Vol. 307, pp. 500–501.

Velázquez, M.; Marucco, J.-F.; Mounaix, P.; Pérez, O.; Ferrier, A. & Moncorgé, R. (2009). Segregation and twinning in the rare-earth-doped KPb_2Cl_5 laser crystals. *Cryst. Growth & Design*, Vol. 9, No.4, pp. 1949-1955.

Vinogradova, N. N.; Galagan, B. I.; Dmitruk, L. N.; Moiseeva, L. V.; Osiko, V. V.; Sviridova, E. E.; Brekhovskikh, M. N. & Fedorov, V. A. (2005). Growth of rare-earth-doped K_2LaCl_5, K_2BaCl_4, and K_2SrCl_4 single crystals. *Inorganic Materials*, Vol. 41, No.6, pp. 654-657.

Virey, E.; Couchaud, M.; Faure, C.; Ferrand, B.; Wyon, C. & Borel, C. (1998). Room temperature fluorescence of $CsCdBr_3$:RE (RE=Pr, Nd, Dy, Ho, Er, Tm) in the 3-5 μm range. *J. All. Comp.*, Vol. 275-277, pp. 311-314.

Voda, M.; Al-Saleh, M.; Lobera, G.; Balda, R. & Fernández, J. (2004). Crystal growth of rare-earth-doped ternary potassium lead chloride single crystals by the Bridgman method. *Opt. Mater.*, Vol. 26, No.4, pp. 359–363.

Vtyurin, A. N.; Isaenko, L. I.; Krylova, S. N.; Yelisseyev, A.; Shebanin, A. P.; Turchin, P. P.; Zamkova, N. G. & Zinenko, V. I. (2004). Raman spectra and elastic properties of KPb_2Cl_5 crystals. *Phys. Stat. Sol. (c)*, Vol. 1, No.11, pp. 3142-3145.

Vtyurin, A. N.; Isaenko, L. I.; Krylova, S. N.; Yelisseyev, A.; Shebanin, A. P. & Zamkova, N. G. (2006). Vibrational spectra of KPb_2Cl_5 and KPb_2Br_5 crystals. *Comp. Mat. Sci.*, Vol. 36, pp. 212-216.

Wang, Y.; Li, J.; Tu, C.; You, Z.; Zhu, Z. & Wu, B. (2007). Crystal growth and spectral analysis of Dy3+ and Er3+ doped KPb_2Cl_5 as a mid-infrared laser crystal. *Cryst. Res. Technol.*, Vol. 42, No.11, pp. 1063-1067.

Zhou, G.; Han, J.; Zhang, S.; Cheng, Z. & Chen, H. (2000). Synthesis, growth and characterization of a new laser upconversion crystal Ba_2ErCl_7. *Prog. Cryst. Growth and Charact. Mater.*, Vol. 40, pp. 195-2000.

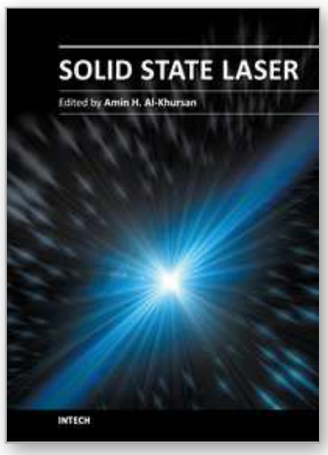

Solid State Laser

Edited by Prof. Amin Al-Khursan

ISBN 978-953-51-0086-7
Hard cover, 252 pages
Publisher InTech
Published online 17, February, 2012
Published in print edition February, 2012

This book deals with theoretical and experimental aspects of solid-state lasers, including optimum waveguide design of end pumped and diode pumped lasers. Nonlinearity, including the nonlinear conversion, up frequency conversion and chirped pulse oscillators are discussed. Some new rare-earth-doped lasers, including double borate and halide crystals, and feedback in quantum dot semiconductor nanostructures are included.

How to reference

In order to correctly reference this scholarly work, feel free to copy and paste the following:

M. Velázquez, A. Ferrier, J.-L. Doualan and R. Moncorgé (2012). Rare-Earth-Doped Low Phonon Energy Halide Crystals for Mid-Infrared Laser Sources, Solid State Laser, Prof. Amin Al-Khursan (Ed.), ISBN: 978-953-51-0086-7, InTech, Available from: http://www.intechopen.com/books/solid-state-laser/rare-earth-doped-low-phonon-energy-halide-crystals-for-mid-infrared-laser-sources

INTECH
open science | open minds

InTech Europe
University Campus STeP Ri
Slavka Krautzeka 83/A
51000 Rijeka, Croatia
Phone: +385 (51) 770 447
Fax: +385 (51) 686 166
www.intechopen.com

InTech China
Unit 405, Office Block, Hotel Equatorial Shanghai
No.65, Yan An Road (West), Shanghai, 200040, China
中国上海市延安西路65号上海国际贵都大饭店办公楼405单元
Phone: +86-21-62489820
Fax: +86-21-62489821

IntechOpen